ACS Catalysis

pubs.acs.org/acscatalysis Research Article

Influence of First and Second Coordination Environment on Structural Fe(II) Sites in MIL-101 for C−H Bond Activation in Methane

Jenny G. Vitillo,* Connie C. Lu, Christopher J. Cramer, Aditya Bhan, and Laura Gagliardi*

Cite This: ACS Catal. 2021, 11, 579−589 Read Online

ACCESS | Metrics & More | Article Recommendations | Supporting Information

ABSTRACT: Divalent iron sites in tri-iron oxo-centered metal nodes in metal−organic frameworks (MOFs) catalyze light alkane oxidation. The first two steps of the reaction sequence, which are also the most energetically demanding ones, are the formation of the active species, Fe(IV)═O, by N_2O decomposition and subsequent C−H bond cleavage. We have employed Kohn−Sham density functional methods to explore how modification of the microenvironment around the Fe(II) center can modulate its catalytic activity, akin to what noted in metalloenzymes. We have varied the substituents on the organic linker of the MIL-101(Fe) MOF, as a way to modulate the energy barriers associated with the first two steps of the methane to methanol reaction. The calculations show that varying substituents has a minimal electronic effect on the iron center and its first coordination shell. However, their proximity to the active site can modify the barriers by 20%. Hydrogen bond donors can lower both barriers, such that the resulting Fe(IV)═O species are simultaneously more stable and more reactive than those of the parent MOF. The screening of a large set of systems allowed us to establish rules for the selection of second coordination shell elements to improve the reactivity of oxoferryl-based catalysts: (i) functionality with a low pK_a or large positive electrostatic potential, (ii) a distance around 1.5 Å between the oxoferryl and any atom of the ring substituent, and (iii) low conformational flexibility of the added substituent.

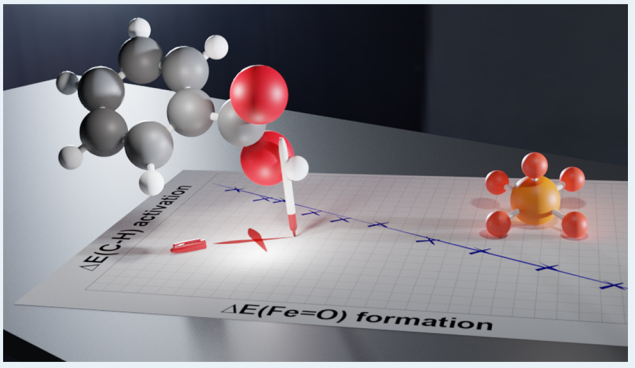

KEYWORDS: *C−H bond activation, MOFs, catalysis, nonheme iron, density functional theory, MIL-101, second shell interactions*

1. INTRODUCTION

Despite decades of active research, the quest for an efficient catalyst for the direct conversion of methane to methanol (MTM) is still ongoing.[1] Di-iron active sites in methane monoxygenases are able to convert methane to methanol selectively at room temperature and atmospheric pressure.[2,3] Among synthetic systems, single Fe(II) sites (α-Fe(II) sites) in iron-based zeolites can hydroxylate methane at room temperature.[2,4,5] Nevertheless, iron centers are hosted as extra framework species in the zeolites pores: this makes them intrinsically disordered, with the copresence of several possible species besides α-Fe(II).[6]

Metal organic frameworks (MOFs) are a class of hybrid organic−inorganic materials characterized by a modular architecture.[7] It is theoretically possible to choose separately the organic (linker) and the inorganic (metal node) components to tailor their structure for a specific application. Additionally, most MOFs are crystalline solids, exhibiting nearly homogeneous physical and chemical properties. All these features place MOFs as catalysts at the boundary between homogeneous and heterogeneous catalysis. MOFs have been demonstrated to be active in C−H bond activation,[8−18] exploiting metal centers hosted in their pores as extra- or intraframework species. While the former present the same problems of heterogeneity of species observed in zeolites, catalytic centers as part of the MOFs framework offer the possibility to tailor more carefully the active sites. The α-Fe(II) sites in zeolites are single iron sites characterized by high-spin ground states and constrained square planar coordination geometries.[2,4,5] It is possible to introduce similar species in a MOF.[11,12,16]

Single, divalent, high spin iron centers mimicking α-Fe(II) sites are hosted in the reduced form of triiron oxo-centered clusters $[Fe(II)Fe(III)_2(\mu_3\text{-}O)]^{6+}$. These clusters are recurrent structural units in many MOFs, including MIL-100 and MIL-101 (MIL, Material of Institute Lavoisier), materials characterized by remarkable chemical and thermal stability.[19−22]

Received: September 7, 2020
Revised: November 22, 2020
Published: December 28, 2020

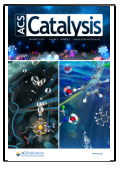

https://dx.doi.org/10.1021/acscatal.0c03906
ACS Catal. 2021, 11, 579−589

Triiron oxo-based MOFs catalyze various reactions involving C−H bond activation.[23−27] We have recently identified them as promising catalysts for the oxidation of methane to methanol and ethane to ethanol, based on Kohn−Sham density functional (KS-DFT) calculations using N_2O as the oxygen source.[28] Simons et al.[16] verified this prediction experimentally, showing that MIL-100(Fe) can catalyze the partial oxidation of propane and ethane. The catalytic cycle for methane is reported in Figure 1. The four steps composing the cycle are (i) N_2O adsorption

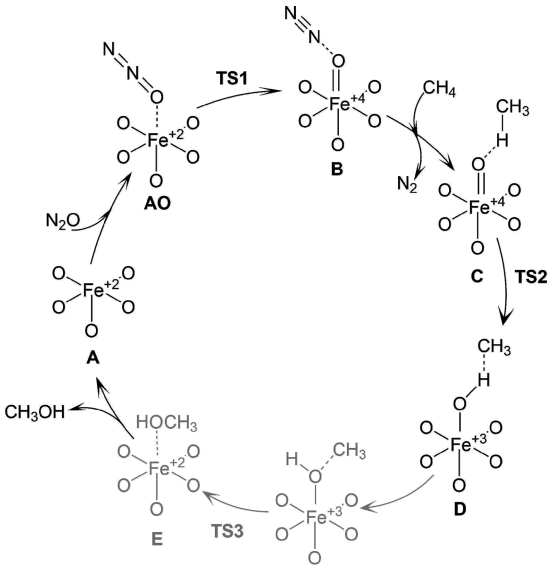

Figure 1. Catalytic cycle for methane to methanol conversion on divalent Fe(II) sites in MIL-101. The part of the cycle considered in the present work is reported in black.

and its decomposition with the formation of the ferryl (from **AO** to **B**), (ii) approach of the alkane and C−H bond cleavage (from **C** to **D**), (iii) radical rebound step with the formation of the alcohol (from **D** to **E**), and (iv) alcohol desorption (from **E** to **A**). The rate-determining step of the reaction is the formation of the ferryl with a barrier (ΔH_{TS1}) of 140 kJ mol^{-1}, while the C−H bond activation enthalpy (ΔH_{TS2}) is 60 kJ mol^{-1} for methane.[28] The radical rebound step is strongly exothermic and almost barrierless, as reported also for other systems.[9,11,13−15,28] The calculations also indicate that the incorporation of heteroatoms in the node,[27−29] such as aluminum and titanium, can decrease the rate determining barrier down to 90 kJ mol^{-1}, in analogy to strategies adopted for bulk (doped) metal oxides[30,31] and zeolites.[32] This behavior was explained through the larger stabilization of the Fe $3d_{z^2}$ orbital by decreasing the spin density on the central oxygen of the cluster ($\rho(O_c)$), in a trans position to the oxo.[5,28] Otherwise, the metal composition in the cluster has no effect on the C−H bond activation step.

The synthesis of mixed metal MOFs presents the challenge of guaranteeing the homogeneity of the metal distribution in all metal nodes.[33,34] Functionalization of the ligand is an alternative approach for tuning the properties of a MOF, having the advantage that the modified material can be often obtained through minimal changes in the pristine synthesis protocols.[35] Gani and Kulik have shown that the catalytic activity for methane to methanol conversion of iron centers in organometallic complexes can be significantly modified by tuning the ligand field strength.[15] Liao et al. reported a similar behavior for ethane oxidation on iron centers in MOFs.[36] In the present work, we used KS-DFT calculations to investigate the effect of various substituents on the linker on the reactivity of Fe(II) centers in triiron oxo-centered clusters (see Figure 2) for the N_2O decomposition and for the methane C−H bond activation steps. Among the triiron oxo-based MOFs, we investigated MIL-101 because its linker, terephthalate, is a suitable platform for the introduction of different functional groups.[35,37] In the first part of the study, we have tested different linkers with the aim to induce electronic changes in the first-coordination shell around Fe(II), similar to those observed upon changing composition of the metal node.[28] The linker has been substituted with several electron-withdrawing and electron-donating groups disposed at the meta-positions to avoid any direct interaction among the ring substituents and Fe(II) active site, the reagents (N_2O and CH_4), or the products (*meta* clusters, see Figure 2a).

Prior studies of Fe-based catalysts[14,15] confirm the generality of the inverse linear relationship between the reaction enthalpies for the formation of the ferryl ($\Delta H_{AO\rightarrow B}$) and the C−H scission ($\Delta H_{C\rightarrow D}$): in other words, more stable ferryl species are less reactive. The presence of noncovalent interactions has been suggested as a way to break this relationship.[14,15] Second-coordination shell interactions are known to influence both the formation and reactivity of heme and nonheme biomimetic metal-oxo complexes[38−40] and MOFs.[41] We have evaluated this effect by considering a second set of clusters (*up* clusters, Figure

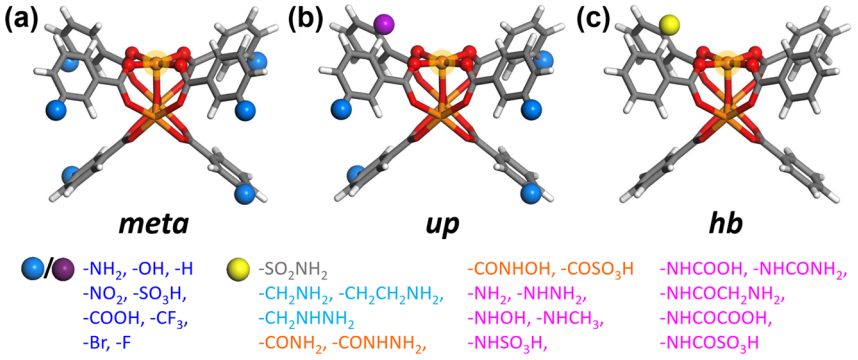

Figure 2. Three sets of clusters used to model the functionalized MIL-101 structures, considering different positioning of the substituents on the phenyl rings. (a) *meta* clusters: $Fe(III)_2Fe(II)(\mu_3\text{-}O)(m\text{-}X\text{-}C_6H_4COO)_6$. (b) *up* clusters: $Fe(III)_2Fe(II)(\mu_3\text{-}O)(o\text{-}X\text{-}C_6H_4COO)(m\text{-}X\text{-}C_6H_4COO)_5$. (c) *hb* clusters: $Fe_2(III)Fe(II)(\mu_3\text{-}O)(o\text{-}L\text{-}C_6H_4COO)(C_6H_5COO)_5$. The group in ortho position in the *up* (purple sphere) and *hb* clusters (yellow sphere) is positioned toward the binding pocket of Fe(II) (orange sphere). Color code: red (oxygen), orange (iron), blue/purple (X group), yellow (L group), gray (carbon), white (hydrogen).

https://dx.doi.org/10.1021/acscatal.0c03906
ACS Catal. 2021, 11, 579−589

2b), where one of the ring substituents points up, toward the Fe(II) center, and then, it can participate directly in the reaction.

Hydrogen bonds (HB) are the most common types of interactions used by biomolecules to determine their functions.[2,42−44] Metalloproteins can switch from catalytic inactivity to autoxidation depending on the number of the HB (and then of HB donor groups) present in the chemical microenvironment around the metal-oxo active site.[2,42,43] Nevertheless, each of the previous studies considered a limited number of systems involving HB donors. It is, then, difficult to draw general conclusions on the basis of the literature data. We have here considered a third set of clusters specifically designed to study the effect of HB on the reactivity of an Fe(II) center (*hb*-clusters, see Figure 2c). This set was designed to evaluate how the different properties of the ligand substituents (acidity, number of possible conformers, size) can determine the efficiency of the group in modulating the reaction profile from **AO** to **D** (see Figure 1).

The results have been leveraged to draw simple rules for the design of new single Fe-catalysts for C−H bond activation. We find that the substituents on the linker induce negligible changes in the electronic properties of the iron and on its first coordination shell. Their presence in the reaction pocket, however, does significantly modify the stability and reactivity of the oxoferryl through noncovalent interactions. The rules derived here are transferrable to catalysts based on other single metal-oxo intermediates.

2. COMPUTATIONAL METHODS

All the calculations were performed using the *Gaussian 16* program.[45] The M06-L[46] density functional in its unrestricted formalism (U) was used in combination with the def2-TZVP basis sets.[47,48] This level of theory has shown to describe accurately the electronic structure of single iron centers in ethane and methane oxidation studies[12] and of the tri-iron oxo-centered cluster[28] when compared to multireference wave function theory. Moreover, it reproduces accurately the experimental activation enthalpy for N_2O decomposition on MIL-100(Fe).[16]

Each of the thirty-six cluster models reported in Figure 2 consists of a $[Fe(II)Fe(III)_2(\mu_3\text{-}O)]^{6+}$ metal node coordinated to six benzoates as in the MIL-101 framework.[49] These linkers were differently functionalized as shown in parts a-c of the same figure. These clusters can be divided in three sets: *meta*- (Figure 2a), *up*- (Figure 2b), and *hb*-clusters (Figure 2c).

For the *meta* and the *up* sets, we introduced electron withdrawing (−F, −Br, −COOH, $-CF_3$, $-SO_3H$, $-NO_2$) and electron donating groups ($-NH_2$, −OH) on the linker as a way to tune the basicity of the first coordination oxygens around the Fe(II) center, and in particular to modulate $\rho(O_c)$. All the phenyl rings have been singly functionalized to maximize the electronic effect of the functional group. The general formula of the clusters is $Fe(III)_2Fe(II)(\mu_3\text{-}O)(m\text{-}X\text{-}C_6H_4COO)_6$, with X = −H, $-NH_2$, −OH, −F, −Br, −COOH, $-CF_3$, $-SO_3H$, or $-NO_2$. In the *meta* clusters, the X groups have been distributed in meta position on the linkers in order to avoid both their mutual interaction and the interaction with the adsorbates (see Figure 2a). The *meta* clusters allow us to evaluate exclusively the electronic influence of the X groups on the catalytic site.

Secondary coordination shell effects have been considered by using the *up* set. They are highly similar to the *meta* set except that a single X group is now in the *ortho* position and directed toward the Fe(II) binding pocket $(Fe(III)_2Fe(II)(\mu_3\text{-}O)(o\text{-}X\text{-}C_6H_4COO)(m\text{-}X\text{-}C_6H_4COO)_5$, see Figure 2b, *up* clusters). This facilitates the direct involvement of the ring substituent in the reaction. We note that even if the *ortho* substituents in the *up* clusters were to point in the opposite direction away from selected Fe active site to follow the reaction, they would still be directed toward another Fe site.

The effect of hydrogen bond on the reaction profile was evaluated specifically using the *hb* cluster (see Figure 2c). The results obtained with the *up* and the *meta* clusters indicated that the electronic effects due to the ring substituents are negligible (see section 3). For this reason, to lower the computational cost associated with the screening, only a single ortho group was introduced per cluster while the other five linkers were kept unfunctionalized. The formula of the *hb* clusters is $Fe_2(III)Fe(II)(\mu_3\text{-}O)(o\text{-}L\text{-}C_6H_4COO)(C_6H_5COO)_5$ (L = $-SO_2NH_2$, $-CH_2NH_2$, $-CH_2CH_2NH_2$, $-CH_2NHNH_2$, $-CONH_2$, $-CONHNH_2$, −CONHOH, $-COSO_3H$, $-NH_2$, $-NHSO_3H$, $-NHCH_3$, $-NHNH_2$, −NHOH, −NHCOOH, $-NHCOCH_2NH_2$, −NHCOCOOH, $-NHCONH_2$, and $-NHCOSO_3H$). Some of these L groups mimic organic moieties found in proteins and have been used for the synthesis of enzyme-MOFs and bio-MOFs.[50,51] Some of the L groups have also been reported to determine enzymatic activity.[2,43] For example, $-CH_2CH_2NH_2$ is essential for the N_2O to N_2 reduction step in bacterial denitrification by nitrous oxide reductase.[2,52,53] The *hb* set covers different acidities and different conformational flexibilities of the L group. The latter has been achieved by selecting as the first moiety of the ring substituent a functionality that is repulsed by the oxygen atoms composing the first coordination shell of Fe(II) (i.e., $-SO_2-$ and −CO−, in the following *hb*-SO_2 and *hb*-CO, respectively) or that can interact with them (i.e., −NH− and $-CH_2-$, in the following *hb*-NH and *hb*-CH_2, respectively) with varying strength. The chain length of the L group was kept to ≤4 moieties to avoid any undesired coordination to the iron center.

Geometry optimizations were carried out by means of the Berny optimization algorithm with analytical gradient. A (99,590) pruned grid was used (i.e., 99 radial points and 590 angular points per radial point). The *meta* clusters in the reagent step (**A** in Figure 1) were carved from the structure reported in ref 49 and they were subjected to a two-step optimization. In the first step (opt-1), the energy convergence threshold was set to 10^{-5} Ha and the positions of all the atoms were optimized, besides those of the six C in position 4, which were kept fixed in the positions occupied in the experimental structure.[49] More stringent convergence criteria in opt-1 resulted in a distorted geometry for some of the clusters that was not representative of the MOF structure. In the second step (opt-2), the positions of all the aryl C atoms and all the S atoms were blocked and *Gaussian 16* default convergence thresholds were set for optimization. Besides the *meta*-**A** cluster, all the other *meta* structures were optimized using only the opt-2 settings. The starting geometry of the *up*-**A** clusters was obtained from the corresponding *meta*-**A** clusters. Their geometry was reoptimized using the opt-2 settings but allowing the free rotation of the *ortho*-functionalized phenyl ring around the C1−C4 axis (i.e., removal of the constraints on C2, C3, C5, and C6 and on the functional group) in order to make the X group free to interact during the reaction. For the *hb* clusters, the starting geometry was obtained from the *up*-H-**A** cluster by functionalizing one of the benzene rings as in Figure 2c. For all the *hb* clusters, we used the same optimization conditions adopted for the *up*-clusters.

https://dx.doi.org/10.1021/acscatal.0c03906
ACS Catal. 2021, 11, 579−589

For all the reaction steps, different starting geometries have been considered especially for the *up* and *hb* clusters, being characterized by several local minima.

All the energetic data have been corrected for the basis set superposition error (BSSE) following the a posteriori method proposed by Boys and Bernardi[54] as implemented in *Gaussian 16*. The BSSE corrected values are indicated by a c superscript and were obtained from the computed Y values as $Y^c = Y + \text{BSSE}$.

Unscaled, harmonic vibrational frequencies were computed analytically. Enthalpies and Gibbs free energies were calculated at 1 atm and 298 K from conventional ideal gas, rigid rotator, particle in a box, quantum mechanical harmonic oscillator partition functions, except that the low vibrational frequencies (<50 cm^{-1}) were replaced by a cutoff value (50 cm^{-1}), following the De Moor scheme[55] to account for limitations in the harmonic oscillator approximation for very low frequency vibrations.[56−60] Charge and spin densities were obtained using Charge Model 5 (CM5)[61] and Hirshfeld population analysis,[62] respectively.

3. RESULTS AND DISCUSSION

In all the studied systems, the ground state electronic configuration is similar in that all the three iron centers are high spin. The most favorable configuration, however, is not the highest possible spin state of the cluster (HS, that is, 1Fe(II)2Fe(III), $2S + 1 = 15$) but the "broken-symmetry" solution where two high-spin Fe(III) centers couple antiferromagnetically for form an intermediate quintet state (BS, $2S + 1 = 5$). This is a common situation in systems having a large multireference character. Although the BS energetics would be more accurate,[16,63] the corresponding wave function is not a spin eigenfunction nor does it have the correct spin density. Because the BS solution is strongly dependent on the initial guess, following the reaction profile for the BS spin state can be cumbersome and hinder both the reproducibility of the present results and comparison among different studies. Following a common strategy,[14,15,63] we simulated all the steps of the reaction on the HS spin surface ($2S + 1 = 15$). In a previous study, we showed that considering the HS solution instead of the BS one introduces only a slight overestimation of the reaction barrier for both N_2O activation and C−H bond scission.[16,28]

Cartesian coordinates for the all the optimized geometries can be found in the Supporting Information and at the Zenodo repository with DOI: 10.5281/zenodo.4256607. All the relevant energetic parameters are reported in Tables S19−S52. The reaction enthalpies and the reaction Gibbs free energies provide an equivalent description of the clusters reactivity. The reaction profiles are discussed in terms of reaction enthalpies in order to allow a direct comparison with the literature data.[9,12,16,28,64] In the discussion, we used for comparison the parent cluster, *up*-H, which features all benzoate linkers and where one of the benzoates was allowed to optimize.

N_2O Activation. This step involves the conversion of **AO** into **B** through the transition state **TS1**, by the decomposition of N_2O on the Fe(II) site with the formation of N_2 and an Fe(IV)═O moiety. This step is the sole kinetically relevant step for all the clusters (see Figures 3 and S1−S4). The benzoates of the *meta*- and *up*-clusters were monosubstituted with groups that can have different electronic effects on the Fe(II) site and its first coordination shell (see bottom part of Figure 3). A more negative charge on the central oxygen of the metal node (O_c) is known to correspond to a lower barrier for N_2O decomposition (ΔH^{C}_{TS1}).[28] Strong electron-donating groups (EDGs), such as

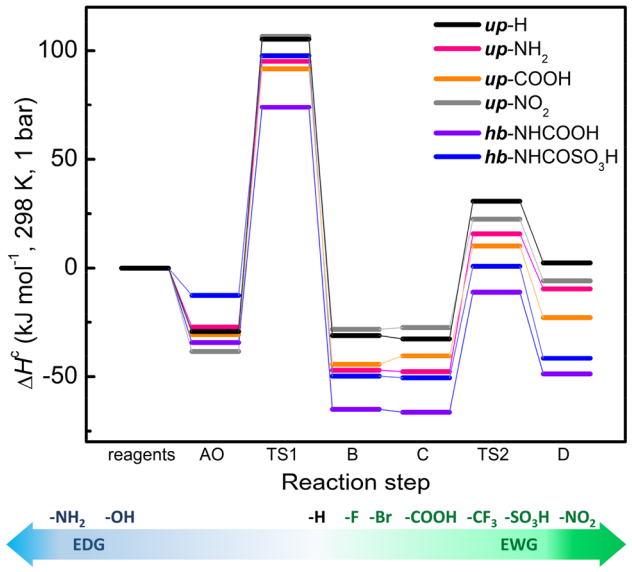

Figure 3. (top) Reaction enthalpies for the activation of methane to methyl radical as computed at the UM06-L/def2-TZVP level following the cycle reported in Figure 2 on the pentadectet spin energy surface for most relevant representatives of the *up*- (*up*-H, *up*-COOH, *up*-NH_2, and *up*-NO_2) and the *hb*-clusters (*hb*-NHCOOH and *hb*-NHCO-SO_3H) taking separated reactants as zero of the enthalpy (data in Tables S19−S51). (bottom) A qualitative scale of the electron donating (EDG) and electron withdrawing (EWG) strength of the X groups.[65]

−NH_2, are expected to increase the electron density on the oxygen atoms in the first coordination shell around Fe(II) and, consequently, decrease ΔH^{C}_{TS1}. Conversely, strong electron-withdrawing groups (EWGs), such as −NO_2, would increase ΔH^{C}_{TS1}. The *meta*-H cluster has a ΔH^{C}_{TS1} of 134.2 kJ mol^{-1}, very close to that previously reported for a similar cluster bearing formate linkers[28] (140.5 kJ mol^{-1}), instead of benzoate linkers. This indicates a negligible influence of the MOF linker electronics and geometry on the reaction profiles. The reaction profiles of the *meta* clusters are also insensitive to the presence of functional groups on the benzoates: they all show similar energy profiles as that for *meta*-H (see Figure S1 and the purple squares in Figure 4). Accordingly, the charge on O_c and Fe in the **A** clusters is independent of the X group (see Tables S1). These results are similar to those reported by Liao et al. for clusters where the iron is coordinated by benzoate anions functionalized with different groups.[36] The slightly larger variation of ΔH_{TS1} observed in ref 36 (10 vs 5 kJ mol^{-1} in the present study) can be associated with the different cluster geometry resulting in a partial exposure of the functional groups in the clusters of Liao et al. Functionalization beyond two atoms from the iron center has also been reported to have no influence on Fe-based reactivity within molecular complexes.[15] As a counterargument, ring substituents in the ortho position have a stronger effect on the electronic properties than those in meta position. In order to investigate if the invariance of the cluster properties on the X groups is associated with their meta position, we tested a control cluster where -NO_2, the strongest EWG, was placed in the ortho position. This cluster is a geometrical isomer of the *up*-NO_2 cluster, except that the −NO_2 points down, away from the Fe(II) site (see Figure S4). The energy profile for this cluster is the same as the one of the *meta*-NO_2. Hence, we can conclude that the ring substituents do not impact the Fe electronics either through delocalization or inductive effects. These findings

https://dx.doi.org/10.1021/acscatal.0c03906
ACS Catal. 2021, 11, 579−589

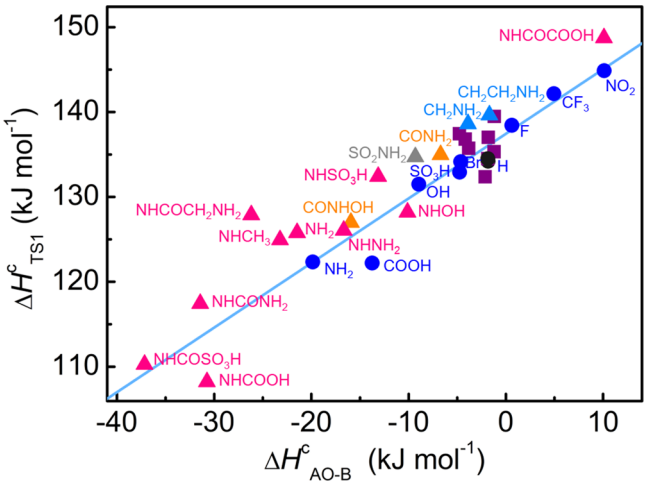

Figure 4. Activation enthalpy, ΔH^C_{TS1}, vs reaction enthalpy for **AO** → **B**, $\Delta H_{AO\rightarrow B}$, at the UM06-L/def2-TZVP level following the cycle reported in Figure 1 for the *meta* (squares, purple), *up* (circles, blue), and *hb* clusters (triangles: *hb*-CH_2, light blue; *hb*-SO_2, gray; *hb*-CO, orange; *hb*-NH, magenta) on the pentadectet spin surface taking separated reactants as zero of the enthalpy (data in Tables S7−S9 and S16−S18). The data point for *up*-H is reported in black to facilitate the comparison. The straight line is obtained by linear fitting of the *up*-clusters points (R^2 = 0.96, residual sum of squares = 5.2), excluding *up*-COOH because it is an outlier.

appear in contrast to what Liao et al.[36] observed in systems where Fe is coordinated by heterocycles, such as pyridine and imidazolate, with observed variations in ΔH_{TS1} as high as 30 kJ mol^{-1}. This difference is mainly associated with systems in which iron is coordinated with the nitrogen of the aromatic ring. This makes iron directly affected by the inductive/delocalization effect on the ring, even if the functional groups that is causing them is more than two atoms away. A different picture is obtained for the *up*-clusters. Here, the reaction profiles are significantly modified by the presence of the X groups (see Figures 3 and S2 and the blue circles in Figure 4). $\Delta H_{AO\rightarrow B}$ spans from 10.1 kJ mol^{-1} for *up*-NO_2 to −19.9 kJ mol^{-1} for *up*-NH_2 while the activation barrier decreases from 144.4 (*up*-NO_2) to 122.2 kJ mol^{-1} (*up*-COOH). The **AO** → **B** step shows a Brønsted−Evans−Polanyi behavior for the *up* series, as evidenced in Figure 4 (light blue line). We previously reported a linear dependence of ΔH^C_{TS1} on $\Delta H_{AO\rightarrow B}$ in a study on MIL-101 metal nodes with different composition.[28] This relation seems to have a general validity: it holds for other nonheme clusters[15] and MOFs.[14] Only *up*-COOH lies slightly off the fitting line.

For the *up* clusters, $\Delta H_{AO\rightarrow B}$ orders as $-NO_2 > -CF_3 > -F > -H > -Br > -SO_3H > -OH > -COOH > -NH_2$ (see Table S8). This ordering *almost* matches the trend based on the EWG/EDG nature of these groups (see the bottom part of Figure 3). We note that the two acidic X groups, −COOH and $-SO_3H$, fall out of the expected order (vide infra). For the *up*-clusters, the electronic charge on O_c, or $q(O_c)$, is constant in **A** (Table S2). In addition, both the Fe(II) electronic charge and Fe(II) spin density in **A** are nearly the same for all the *up* clusters (see Table S2), as well as the Fe(IV) electronic charge and spin density in **B** (Table S8). This is in agreement with the results from the *meta*-clusters. Hence, we can rule out any electronic inductive effect of the X groups as the cause for the significant change in the reactivity of the iron center in the *up*-clusters.

One parameter that does vary among the *up*-clusters is the spin density of the O_{oxo} ($\rho(O_{oxo})$, see Table S5) in **B**. Moreover, a linear relationship was observed between $\Delta H_{AO\rightarrow B}$ and $\rho(O_{oxo})$ for all X groups, with the exception of −COOH and $-SO_3H$ (see Figure S8). A linear relationship also exists between $\Delta H_{AO\rightarrow B}$ and the ferryl bond length, d(Fe−O_{oxo}) (see Figure S8), where the slope is negative. d(Fe−O_{oxo}) and $q(O_{oxo})$ are often used as descriptors for the ferryl stability in the literature.[5,14,41,43] Although, the range spanned by both d(Fe−O_{oxo}) and $q(O_{oxo})$ for the *up*-clusters is very small, linear scaling relationships between $\Delta H_{AO\rightarrow B}$ and d(Fe−O_{oxo}) or $\rho(O_{oxo})$ have been reported for other MOFs.[14,41]

By inspecting the structures of **B** for the *up*-clusters, it becomes evident that X-group and the Fe(IV)═O form noncovalent interactions (see Figures 5 and S7 for *up*-COOH

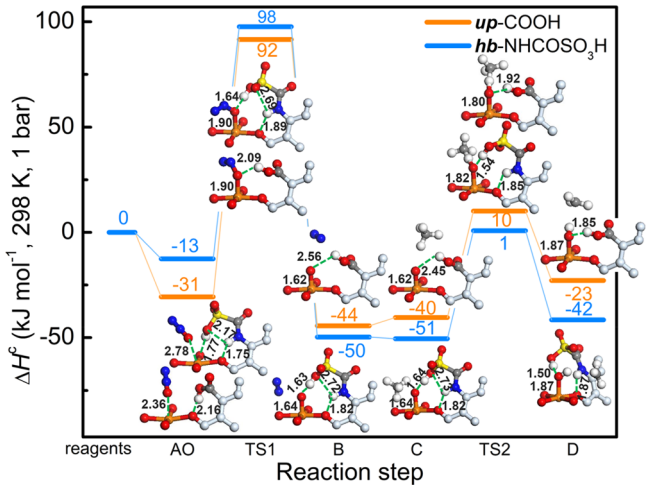

Figure 5. Reaction profiles for the C−H bond activation in methane catalyzed by the best candidate among the *up*- (*up*-COOH, orange) and *hb*-clusters (*hb*-$NHCOSO_3H$, light blue), as calculated at the UM06-L/def2-TZVP level following the cycle reported in Figure 1 on the pentadectet spin energy surface. Separated reactants are set as zero of the enthalpy. The optimized structure of the Fe center and its first coordination sphere, and the interacting −COOH/$-NHCOSO_3H$ functional group is shown for each step. Color code: red (oxygen), orange (iron), blue (nitrogen), yellow (sulfur), gray (carbon), white (hydrogen), general framework atoms (light blue).

and *up*-SO_3H, respectively). Hydrogen bond donors should stabilize Fe(IV)═O since $q(O_{oxo})$ is partially negative (see Scheme 1 and Table S8) and thereby lower $\Delta H_{AO\rightarrow B}$. Accordingly, the four groups with the lowest ΔH^C_{TS1} (−SO_3H,

Scheme 1. Noncovalent Interactions as Hydrogen Bond Can Stabilize the Different Intermediates of the Reaction Reported in Figure 1[a]

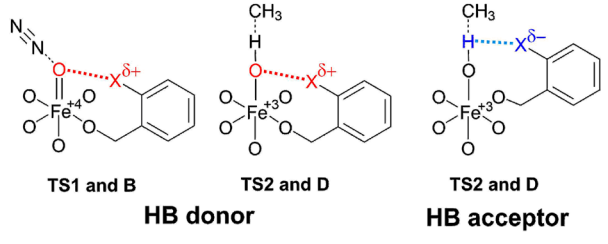

[a]The cases of (left) a hydrogen bond donor and (right) a hydrogen bond acceptor as the ring substituent are schematized.

https://dx.doi.org/10.1021/acscatal.0c03906
ACS Catal. 2021, 11, 579−589

−OH, −COOH, and $-NH_2$) are all hydrogen bond donors. On the other hand, groups that are negatively charged should destabilize Fe(IV)═O, raising ΔH^{C}_{TS1}. For this reason, *up*-NO_2 has the highest ΔH^{C}_{TS1} among the *up*-clusters. The electrostatic potential (ESP) maps of **B** for *up*-COOH and *up*-NO_2 in Figure S13 show that these X groups can significantly decrease and increase, respectively, the negative ESP region surrounding the oxo group. Otherwise, the charge on the carboxylates remains essentially unchanged upon functionalization of the phenyl. In the plots in Figure S8, the two clusters having the strongest HB donor group, *up*-COOH and *up*-SO_3H, fall out of the trend. The proton of the group engages the oxoferryl in a strong hydrogen bond in **B** (see Figure 5 and S7 for *up*-COOH and *up*-SO_3H, respectively), causing a significant modification both of d(Fe−O_{oxo}) and $q(O_{oxo})$ with respect to the parent cluster.

Despite the significant role of hydrogen-bonding in **B**, the observed trend in ΔH^{C}_{TS1} among the HB donors (NH_2 < −COOH < −OH < $-SO_3H$) does not follow the trend expected on the basis of pK_a ($-SO_3H$ < −COOH < $-NH_2$ < −OH).[66] This lack of correlation stems from the interaction of the HB donors not only with the oxylferryl in **TS1** and **B** but also with the MOF carboxylate O-donors in **A** and **AO**. The latter interaction increases the stability of **AO**, which raises ΔH^{C}_{TS1}. Moreover, the conformation of the HB-donors can change significantly from **A**/**AO** to **TS1**/**B**. For X = $-NH_2$ and −OH, the changeover in the HB acceptor during **AO** → **TS1** does not require a change in the X group position. On the other hand, a major reorganization of the X group is observed for both $-SO_3H$ and −COOH. Breaking the HB interaction between the HB donor and the MOF framework in **AO** results in an energy penalty that can partly or fully negate any favorable stabilization of the ferryl species. For *up*-SO_3H, the strongest HB donor in the *up* set, the energy penalty is so large that the overall energy profile is on par to that of the parent cluster, *up*-H. An examination of the **AO** structure for *up*-SO_3H shows a short H-bond distance between $-SO_3H$ and the MOF framework (d(SO_3H···OOC) = 1.87 Å). A conformer of *up*-SO_3H-**A** with no HB is less stable by 24 kJ mol^{-1}, which we consider as an estimate of the strength of the H-bond. In **TS1**, the new HB distance between $-SO_3H$ and the forming oxoferryl is similarly short, d(SO_3H ···O═Fe) = 1.78 Å. Hence, any benefit derived from HB to $-SO_3H$ in **TS1** is essentially canceled out. On the other hand, −COOH has both a higher pK_a than $-SO_3H$ and a longer HB distance in **AO**, d(COOH···OOC), of 2.16 Å. This gives a significantly lower energy penalty of only 3 kJ mol^{-1}. Coupled to the formation of a strong HB interaction in **TS1** (d(COOH···O═Fe) = 2.089 Å, estimated to be 20 kJ mol^{-1}), *up*-COOH has the second lowest ΔH^{C}_{TS1} of the *up*-clusters set.

Moving beyond the *up*-clusters, we designed a third set of models, the *hb*-clusters (Figure 2), to investigate more complex HB-donors, which are labeled as L groups. The *hb*-clusters are simplified in that only a single linker is functionalized with the L group in the ortho position, while the other five linkers are simple benzoates. Indeed, the similarity of the results for *up*-NH_2 and *hb*-NH_2 (see Figure 4) further demonstrates that only functionalities directed toward the Fe binding pocket have an effect on the reaction energy profile. The L groups can be further categorized into four subsets according to their different linkages, which are depicted using the color code shown in Figure 2: $-SO_2-$ (gray), $-CH_2-$ (light blue), −CO− (orange), and −NH− (magenta). Of these 18 total L groups, only the data for 15 L groups are presented. The energetics obtained for the *hb*-clusters are reported in Figure S3 and as triangles in Figure 4. Three L groups ($-CH_2NHNH_2$, $-CONHNH_2$, and $-COSO_3H$) were eschewed from the analyses because they form coordinate bonds to the Fe(II) center in **A** (<2.4 Å), which precludes N_2O binding and formation of **AO**.

For the *hb* set, the effect of the functional group on **AO** → **B** is even greater than that observed for the *up* set (see Figure 4). Most L groups in the *hb* set possess multiple HB donors, and all L groups have at least one. Based on that, it can be expected that $\Delta H_{AO\rightarrow B}$ will be lower or equal to the parent cluster one. This is actually verified for all the *hb*-clusters, with the exception of *hb*-NHCOCOOH, which has a significantly larger $\Delta H_{AO\rightarrow B}$ (see Figure 4). The $\Delta H_{AO\rightarrow B}$ value spans from 10.1 kJ mol^{-1} for *hb*-NHCOCOOH to −37.2 kJ mol^{-1} for *hb*-$NHCOSO_3H$ while the activation barrier decreases from 148.7 (*hb*-NHCOCOOH) to 108.2 kJ mol^{-1} (*hb*- NHCOOH). A characteristic Brønsted−Evans−Polanyi correlation between $\Delta H_{AO\rightarrow B}$ and ΔH^{C}_{TS1} is also observed for the *hb* set, with all the points lying close to the same fitted line as that for the *up* set (see Figure 4).

Similar to the *up*-clusters, the energy ordering of ΔH^{C}_{TS1} for the *hb*-clusters does not follow any pK_a trend. For example, *hb*-$NHSO_3H$ and *hb*-$NHCOSO_3H$ both terminate with the very acidic $-SO_3H$ moiety that coordinates the MOF framework in **AO** and the ferryl in **TS1** and in **B** (see Figure 5). Nevertheless, *hb*-$NHSO_3H$ has a ΔH^{C}_{TS1} almost coincident to the parent cluster, while *hb*-$NHCOSO_3H$ has a ΔH^{C}_{TS1} that is 24 kJ mol^{-1} lower. Again, the differing conformational changes in the L group from **AO** to **TS1**/**B** account for this energy difference (see below). The complexity of the L groups also result in varying flexibility (or rigidity) that is not trivial to predict a priori. For example, *hb*-NHCOCOOH, despite having an acidic proton, is unable to form a stabilizing HB interaction with the oxoferryl unit. Instead, the −NHCOCOOH group engages in a strong internal HB between the underlined atoms that form a stable 5-membered ring. One consequence of this internal HB is that the δ^- CO subunit is directed toward the oxoferryl unit (while the δ^+ OH is directed away), which destabilizes **TS1**/**B** and results in the highest ΔH^{C}_{TS1} and $\Delta H_{AO\rightarrow B}$ among the *hb* set.

The lowest $\Delta H_{AO\rightarrow B}$ is obtained for *hb*-$NHCOSO_3H$, and this L group demonstrates several beneficial traits beyond its low pK_a. An important feature is the rigid amide bond, which helps create a network of H-bonds involving the L group, the MOF carboxylate O-donors, and the oxyferryl (see Figure 6). In **AO**, the HB network comprises 3 interactions: (i) −NH···MOF, (ii) $-SO_3H$···MOF, and (iii) $-NHCOSO_2OH$, where an internal HB between the underlined atoms forms a 5-membered ring (see Figure 6). All three HB interactions are quite strong in **AO**, with short distances of 1.75, 1.77, and 2.17 Å, respectively.[67] However, these 3 HB interactions evolve differently during the reaction.

For *hb*-$NHCOSO_3H$, the strong HB between −NH− and the MOF is maintained throughout the reaction from **AO** to **D**. The SO_3H···MOF H-bond breaks as a SO_3H···O═Fe H-bond forms during the reaction from **AO** to **TS1**/**B**. Other clusters that incorporate SO_3H, such as *up*-SO_3H and *hb*-$NHSO_3H$, show a similar changeover in the HB acceptor as *hb*-$NHCOSO_3H$ but have significantly greater ΔH^{C}_{TS1} barriers. Hence, the favorable energetics for *hb*-$NHCOSO_3H$ is mainly attributed to the internal H-bond. The internal H-bond, coupled with the rigidity of the amide linkage and the −NH···MOF interaction, forces the SO_3H moiety to point toward the Fe binding pocket. Also, this internal H-bond relaxes significantly from 2.17 Å in **AO** to 2.69 Å in **TS1**, during which the SO_3H shifts its HB acceptor from the MOF to the oxoferryl unit. The elongation of this internal HB

https://dx.doi.org/10.1021/acscatal.0c03906
ACS Catal. 2021, 11, 579−589

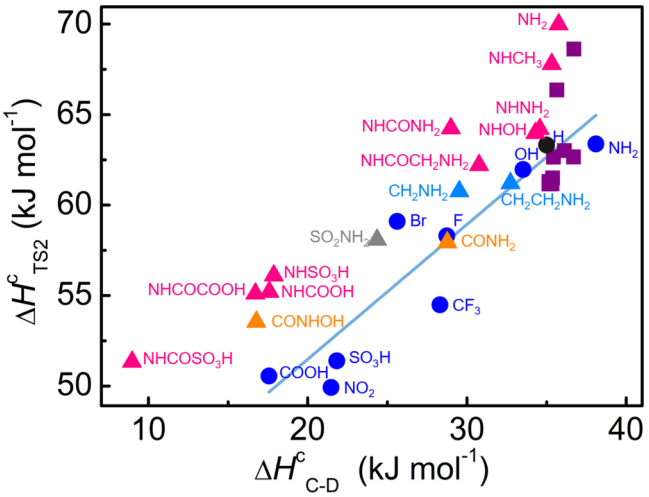

Figure 6. Activation enthalpy, ΔH^C_{TS2}, vs the reaction enthalpy for **C** → **D**, $\Delta H_{C\to D}$, at the UM06-L/def2-TZVP level following the cycle reported in Figure 1 for the *meta* (squares, purple), *up* (circles, blue), and *hb* clusters (triangles *hb*-CH$_2$, light blue; *hb*-SO$_2$, gray; *hb*-CO, orange; *hb*-NH, magenta) on the pentadectet spin surface taking separated reactants as zero of the enthalpy (data in Tables S10−S12 and S16−S18). The data point for *up*-H is reported in black to facilitate the comparison. The blue line is obtained by linear fitting of the *up* clusters data (R^2 = 0.83, residual sum of squares = 34).

distance also releases strain in the **AO** structure, which helps compensate the loss of the SO$_3$H···MOF H-bond in **TS1**.

Collectively, the *hb*-cluster series highlights the importance of L groups with multiple H-bonding partners such that a HB network can engage and respond dynamically to the active site as the reaction progresses. The optimal L groups destabilize **AO** while stabilizing **B** via a H-bond to the forming oxoferryl, akin to the *up*-clusters. Destabilization of **AO** occurs when the L group can partially occlude the Fe(II) binding site, so as to weaken N$_2$O binding and raise the energy of **AO**, but not to shut out N$_2$O. In other words, an L group can influence positively the reaction only if any atom of the L group is not too close but also not too far from the position that will be occupied by O$_{oxo}$ (located about 1.6 Å above the Fe^{2+} center). Without wanting to be strict, we could indicate 1.5 Å as an optimal value for the distance of a HB donor from O$_{oxo}$ to have a more favorable reactivity.

C−H Bond Activation. The **C** → **D** reaction step corresponds to homolytic C−H bond cleavage, that is the abstraction of a hydrogen radical from methane by the oxoferryl (**C**) resulting in the formation of a methyl radical and a Fe(III)−OH (**D**). The corresponding transition state is **TS2**. Again, both the reaction enthalpy ($\Delta H_{C\to D}$) and the activation enthalpy (ΔH^C_{TS2}) are very similar for all the *meta* clusters. Accordingly, all the ferryl species in the set are identical based on their hydrogen affinity (E_H),[43,68,69] and on their electronic and geometrical properties (see Tables S4 and S10).[5,14,43]

For the *up* and *hb* sets, the direct interaction of the functional group with the intermediates is expected to influence the energetics of C−H bond scission. Fe(III)−OH is both a HB donor and a HB acceptor. Thus, for the **C** → **D** step, any X/L group that is a HB donor or acceptor can facilitate C−H bond scission. For HB donor groups (or positively charged), their preexisting HB to the oxo is expected to strengthen in going from Fe(IV)═O to Fe(III)−OH because of the increased polarity in the O atom (see left part of Scheme 1). For HB acceptor groups (or negatively charged) the stabilization of **D** would happen through the formation of a new HB (see right part of Scheme 1).

Indeed, the presence of the functional group in close proximity to the oxoferryl significantly influences the **C** → **D** step for both the *up* and *hb* sets (circles and triangles in Figure 6, respectively). For the *up*-clusters (Tables S5, S11, and S17), a Brønsted−Evans−Polanyi correlation is observed (blue line in Figure 6). The *hb* clusters (Tables S6, S12, and S18) follow roughly this same trend (although slightly moved upward). Among the descriptors,[5,14,43,68,69] only the hydrogen-atom affinity, E_H, shows a linear relationship with $\Delta H_{C\to D}$ and ΔH^C_{TS2} (see Figures S11 and S12). The failure of other descriptors, for example, d(Fe−O$_{oxo}$), ρ(O$_{oxo}$) (Figures S8−S9), stresses the influence of several contemporaneous factors (hydrogen bond, oxygen basicity, acidity of the functional group, etc.) in determining the reaction energy. Because E_H implicitly includes most of these factors, then it is not surprising that E_H has been proven to be a useful descriptor for ΔH^C_{TS2} across many different catalysts.[43,68,69]

All the *up*-clusters have a lower ΔH^C_{TS2} than *up*-H, except *up*-NH$_2$, which has an equal ΔH^C_{TS2} (63 kJ mol^{-1}). The lowest barrier for the *up* set is calculated for *up*-NO$_2$ (50 kJ mol^{-1}). Most of the *hb*-clusters have a lower ΔH^C_{TS2} than *up*-H. The lowest ΔH^C_{TS2} is obtained in this set for *hb*-NHCOSO$_3$H, which is also the cluster having the lowest barrier for the ferryl formation (see Tables S7−S12). The reasons behind this low ΔH^C_{TS2} are the same identified for ΔH^C_{TS1}, and in particular, the further relaxation of the very constrained geometry of the −NHCOSO$_3$H group going from **C** to **D** (see Figure 5). Interestingly, ΔH^C_{TS2} calculated for methane in the *up*-COOH, *up*-SO$_3$H, *up*-NO$_2$, and *hb*-NHCOSO$_3$H are only 10 kJ mol^{-1} higher than those calculated for ethane on the unfunctionalized MOF (39 kJ mol^{-1}).[28]

Although both HB donors and HB acceptors can decrease the enthalpy for the C−H bond cleavage, the way they do it, can influence the selectivity of the reaction. Scheme 1 illustrates the different HB interactions that are possible in **D**. The calculations evidence an important consequence of this difference. For HB donors, the methyl radical interacts with the H atom of Fe(III)−OH in **D**. However, an HB acceptor can also interact with the H atom of the Fe−OH, forcing the methyl radical to decoordinate. This generates a more stable conformer of **D**, labeled **D′**, where the methyl radical is removed from the reaction site (see section S8 and Figure S5). It is evident that **D′** can favor the reaction of the methyl with the framework or with other species adsorbed in the framework (e.g., other methyl radicals to make C$_2$H$_6$ from CH$_3$* + CH$_3$* → C$_2$H$_6$) over methanol production.

Functional groups possessing both an HB donor and HB acceptor can have multiple **D**/**D′** structures that although very similar in energy, exhibit very different geometries. One of them is *up*-COOH: the −OH moiety is a HB donor, while −C═O is a HB acceptor. In Figure 5, the −OH moiety interacts with the O atom in Fe(III)−OH, while the H atom interacts with the methyl radical. An alternate conformer of **D** exists (Figure S6) where the −C═O interacts with the H atom in Fe(III)−OH. Here, the fortuitous interaction of the −OH moiety with the methyl radical prevents its escape from the reaction site (see Figure S6). In summary, while a sole HB acceptor may negatively impact reaction selectivity by allowing for methyl radical escape, an additional HB donor can "capture" the methyl radical in the reaction site.

https://dx.doi.org/10.1021/acscatal.0c03906
ACS Catal. 2021, 11, 579−589

Selection of the Catalyst. It is generally accepted that, comparing similar systems, species that have a higher enthalpy of formation are more stable and then less reactive. This concept underlies the well-established inverse linear relationship between ΔH^{C}_{TS2} and $\Delta H_{AO\rightarrow B}$[14,70] and between $\Delta H_{C\rightarrow D}$ and $\Delta H_{AO\rightarrow B}$.[15] Here, the noncovalent interactions clearly breaks this trend as shown in Figures 7 and S10, respectively, which

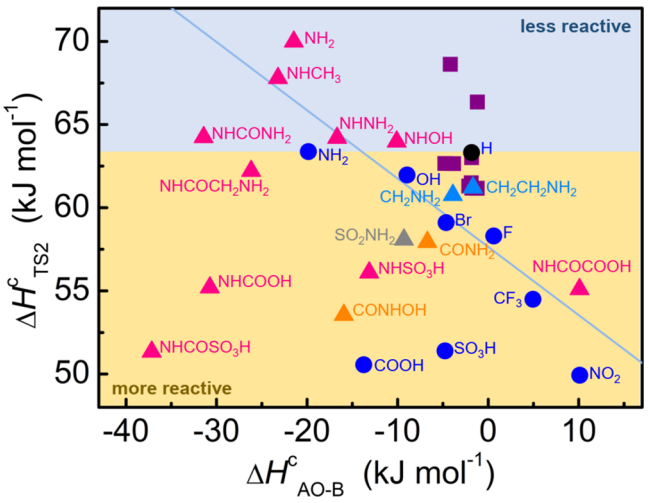

Figure 7. Activation enthalpy for **C** → **D**, ΔH^{C}_{TS2}, vs the reaction enthalpy for **AO** → **B**, $\Delta H_{AO\rightarrow B}$, at the UM06-L/def2-TZVP level following the cycle reported in Figure 1 for the *meta* (squares, purple), *up* (circles, blue), and *hb* clusters (triangles *hb*-CH_2, light blue; *hb*-SO_2, gray; *hb*-CO, orange; *hb*-NH, magenta) on the pentadectet spin surface taking separated reactants as zero of the enthalpy (data in Tables S10–S12 and S16–S18). The data point for *up*-H is reported in black to facilitate the comparison. The graph is divided in two areas: ferryls more reactive (orange background) and less reactive (blue background) than *up*-H, respectively. The blue line is obtained by linear fitting of all the *up* clusters besides *up*-COOH and *up*-SO_3H (R^2 = 0.63, residual sum of squares = 45).

clearly do not follow any linear correlation.[14,15] In Figure 7, the plot of ΔH^{C}_{TS2} versus $\Delta H_{AO\rightarrow B}$ is divided into two parts separated by *up*-H (black dot). Clusters in the top part (blue shade) are more reactive to CH_4 relative to *up*-H, while clusters in the bottom part (orange shade) are less reactive.

A majority of the *up*-clusters, X= $-NH_2$, $-OH$, $-F$, $-Br$, and $-CF_3$, do follow a linear relation (see light blue line in Figure 7). Notably, this line does not include *up*-H (black dot) nor *up*-COOH, *up*-SO_3H, and *up*-NO_2. Likewise, most of the *hb* clusters lie very close to the *up* cluster line but there are several exceptions, in particular: *hb*-NHCOOH, *hb*-$NHSO_3H$, *hb*-CONHOH, and *hb*-$NHCOSO_3H$. The clusters that significantly deviate from the linear trend, all form a strong HB to Fe(III)−OH (see Figures 5 and S7). These results prove that catalysts with HB donors require milder conditions for both N_2O and CH_4 activation, so this is a design principle to achieve more favorable formation energy and greater reactivity at the same time.

The rate-determining step for all the clusters is the N_2O activation. The selection of the most promising catalyst should consider then $\Delta H_{AO\rightarrow B}$ (or ΔH^{C}_{TS1}) as the preferred parameter. The majority of the clusters showed a more exothermic **AO** → **B** step than *up*-H. Using this criteria, we target *up*-COOH and *up*-NH_2 from the *up* set, as well as *hb*-$NHCOSO_3H$ and *hb*-NHCOOH from the *hb* set, as the next-generation MIL-based catalysts. Among them, only MIL-101-NH_2(Fe) has already been synthesized.[71,72] While MIL-101-COOH could be obtained through a direct synthesis (in analogy to its chromium analogues),[73] the high reactivity of the $-NHCOSO_3H$ and −NHCOOH functionalities would make necessary the use of postsynthesis procedures to obtain the corresponding MOFs. Peptide-functionalized MIL-101 materials can be synthesized by leveraging the presence of amino groups in MIL-101-NH_2.[50] Amino groups in MOFs can also be converted to isocyanate through a soft synthesis procedure,[74] where isocyanate is an even more flexible platform for postsynthesis modification of the organic linker. The syntheses reported for −NHCOOH and $-NHCOSO_3H$ require amino or isocyanate functionalized phenyl as reagents.[75−7775] These protocols can be used as a starting point for the synthesis of MIL materials hosting the *hb*-$NHCOSO_3H$ and *hb*-NHCOOH active sites. Additionally, issues related to the stability of −NHCOOH and $-NHCOSO_3H$ in the pressure and temperature conditions adopted to run the methane to methanol reaction, that are outside the aim of the present work, should also be considered in future experimental studies.

4. CONCLUSIONS

Delocalization/inductive effects on the linker are found to insignificantly impact the reaction profiles for methane oxidation catalyzed by Fe species in MIL-101(Fe). Indeed, the monosubstitution of the linkers has little influence on the electronic properties of the $[Fe(II)Fe_2(III)(\mu_3\text{-}O)]^{6+}$ metal node and its first coordination sphere, independent of whether electron-withdrawing or electron donating groups are used.

A completely different scenario is predicted when the substituting functional group can engage in noncovalent interactions with species in the reaction environment. We found that the presence of both hydrogen bond donors and acceptors on the substituent can lower the activation energy for the C−H bond scission. However, only hydrogen bond *donors* (or, more generally, centers presenting a partial positive charge) decrease the barrier for the rate-determining step of the reaction, N_2O decomposition, by engaging the oxoferryl in a hydrogen bond. This is another illustration of the parallels between MOFs and enzymes because hydrogen bonds are pivotal in determining the function in many examples of the latter.[43]

The screening of twenty-six catalyst candidates identified key factors beyond proton acidity and proximity to the reaction center that should be considered when introducing substituent functional groups. In particular, one complication is that atoms characterized by partial negative charges in the first coordination sphere of the Fe(II) site (e.g., the O atoms of the carboxylates in MILs) can also engage HB donors in a strong hydrogen bond. Thus, single HB donors must partition between HB interactions with the framework and the oxoferryl species. The energy difference diminishes the stabilization of the HB with Fe(IV)═O. We found that more rigidly constrained HB donors can mitigate this consideration. Another factor affecting functional group utility is its distance from the Fe center: the group should be as close as possible to the reaction center so long as does not interfere with the catalytic cycle by coordinating the Fe(II) site itself (substituent to oxoferryl distance ∼1.5 Å).

The negligible electronic effect on the metal node of linker substitution has qualitative implications for iron species found in other carboxylate-based MOFs and likely as well for other homogeneous and heterogeneous metal-oxo based catalysts for oxidation reactions. The synthesis of catalysts placing −COOH,

https://dx.doi.org/10.1021/acscatal.0c03906
ACS Catal. 2021, 11, 579−589

$-NH_2$, $-NHCOSO_3H$, or $-NHCOOH$ species in proximity to reactive metal center is particularly encouraged. The models here studied neglect the mutual interactions among functional groups on different phenyls and they can be representative models only for MOFs where a minor fraction of the linkers is functionalized. Future computational studies should be directed to evaluate how these interactions modify the Fe reactivity in highly functionalized MILs.

■ ASSOCIATED CONTENT

Supporting Information

The Supporting Information is available free of charge at https://pubs.acs.org/doi/10.1021/acscatal.0c03906.

Relevant geometrical, electronic, and energetic parameters for all the structures and additional energetic plots (PDF)

Cartesian coordinates for all the optimized geometries (ZIP)

■ AUTHOR INFORMATION

Corresponding Authors

Jenny G. Vitillo − *Department of Chemistry, Chemical Theory Center, and Supercomputing Institute, University of Minnesota, Minneapolis, Minnesota 55455-0431, United States; Department of Science and High Technology and INSTM, Università degli Studi dell'Insubria, I-22100 Como, Italy;* orcid.org/0000-0002-6213-2039; Email: jg.vitillo@gmail.com

Laura Gagliardi − *Department of Chemistry, Pritzker School of Molecular Engineering, James Franck Institute, University of Chicago, Chicago, Illinois 60637, United States;* orcid.org/0000-0001-5227-1396; Email: lgagliardi@uchicago.edu

Authors

Connie C. Lu − *Department of Chemistry, Chemical Theory Center, and Supercomputing Institute, University of Minnesota, Minneapolis, Minnesota 55455-0431, United States;* orcid.org/0000-0002-5162-9250

Christopher J. Cramer − *Department of Chemistry, Chemical Theory Center, and Supercomputing Institute, University of Minnesota, Minneapolis, Minnesota 55455-0431, United States;* orcid.org/0000-0001-5048-1859

Aditya Bhan − *Department of Chemical Engineering and Materials Science, University of Minnesota, Minneapolis, Minnesota 55455, United States;* orcid.org/0000-0002-6069-7626

Complete contact information is available at: https://pubs.acs.org/10.1021/acscatal.0c03906

Notes

The authors declare no competing financial interest.

■ ACKNOWLEDGMENTS

This work was supported by the Inorganometallic Catalyst Design Center, an EFRC funded by the DOE, Office of Basic Energy Sciences (DE-SC0012702). The authors acknowledge the Minnesota Supercomputing Institute (MSI) at the University of Minnesota for providing computational resources.

■ REFERENCES

(1) Sushkevich, V. L.; Palagin, D.; Ranocchiari, M.; van Bokhoven, J. A. Selective anaerobic oxidation of methane enables direct synthesis of methanol. *Science* **2017**, *356*, 523−527.

(2) Snyder, B. E. R.; Bols, M. L.; Schoonheydt, R. A.; Sels, B. F.; Solomon, E. I. Iron and Copper Active Sites in Zeolites and Their Correlation to Metalloenzymes. *Chem. Rev.* **2018**, *118*, 2718−2768.

(3) Zecchina, A.; Califano, S. In *The Development of Catalysis*; John Wiley & Sons, Inc., 2017; pp 269−298.

(4) Snyder, B. E. R.; Böttger, L. H.; Bols, M. L.; Yan, J. J.; Rhoda, H. M.; Jacobs, A. B.; Hu, M. Y.; Zhao, J.; Alp, E. E.; Hedman, B.; et al. Structural characterization of a non-heme iron active site in zeolites that hydroxylates methane. *Proc. Natl. Acad. Sci. U. S. A.* **2018**, *115*, 4565−4570.

(5) Snyder, B. E. R.; Vanelderen, P.; Bols, M. L.; Hallaert, S. D.; Böttger, L. H.; Ungur, L.; Pierloot, K.; Schoonheydt, R. A.; Sels, B. F.; Solomon, E. I. The active site of low-temperature methane hydroxylation in iron-containing zeolites. *Nature* **2016**, *536*, 317.

(6) Zecchina, A.; Rivallan, M.; Berlier, G.; Lamberti, C.; Ricchiardi, G. Structure and nuclearity of active sites in Fe-zeolites: comparison with iron sites in enzymes and homogeneous catalysts. *Phys. Chem. Chem. Phys.* **2007**, *9*, 3483−3499.

(7) Zhou, H.-C.; Long, J. R.; Yaghi, O. M. Introduction to Metal−Organic Frameworks. *Chem. Rev.* **2012**, *112*, 673−674.

(8) Manna, K.; Ji, P.; Lin, Z.; Greene, F. X.; Urban, A.; Thacker, N. C.; Lin, W. Chemoselective single-site Earth-abundant metal catalysts at metal−organic framework nodes. *Nat. Commun.* **2016**, *7*, 12610.

(9) Vogiatzis, K. D.; Haldoupis, E.; Xiao, D. J.; Long, J. R.; Siepmann, J. I.; Gagliardi, L. Accelerated Computational Analysis of Metal−Organic Frameworks for Oxidation Catalysis. *J. Phys. Chem. C* **2016**, *120*, 18707−18712.

(10) Beyzavi, M. H.; Vermeulen, N. A.; Howarth, A. J.; Tussupbayev, S.; League, A. B.; Schweitzer, N. M.; Gallagher, J. R.; Platero-Prats, A. E.; Hafezi, N.; Sarjeant, A. A.; et al. A Hafnium-Based Metal−Organic Framework as a Nature-Inspired Tandem Reaction Catalyst. *J. Am. Chem. Soc.* **2015**, *137*, 13624−13631.

(11) Xiao, D. J.; Bloch, E. D.; Mason, J. A.; Queen, W. L.; Hudson, M. R.; Planas, N.; Borycz, J.; Dzubak, A. L.; Verma, P.; Lee, K.; et al. Oxidation of ethane to ethanol by N_2O in a metal−organic framework with coordinatively unsaturated iron(II) sites. *Nat. Chem.* **2014**, *6*, 590−595.

(12) Verma, P.; Vogiatzis, K. D.; Planas, N.; Borycz, J.; Xiao, D. J.; Long, J. R.; Gagliardi, L.; Truhlar, D. G. Mechanism of Oxidation of Ethane to Ethanol at Iron(IV)−Oxo Sites in Magnesium-Diluted Fe_2(dobdc). *J. Am. Chem. Soc.* **2015**, *137*, 5770−5781.

(13) Osadchii, D. Y.; Olivos-Suarez, A. I.; Szécsényi, Á.; Li, G.; Nasalevich, M. A.; Dugulan, I. A.; Crespo, P. S.; Hensen, E. J. M.; Veber, S. L.; Fedin, M. V.; et al. Isolated Fe Sites in Metal Organic Frameworks Catalyze the Direct Conversion of Methane to Methanol. *ACS Catal.* **2018**, *8*, 5542−5548.

(14) Rosen, A. S.; Notestein, J. M.; Snurr, R. Q. Structure−Activity Relationships That Identify Metal−Organic Framework Catalysts for Methane Activation. *ACS Catal.* **2019**, *9*, 3576−3587.

(15) Gani, T. Z. H.; Kulik, H. J. Understanding and Breaking Scaling Relations in Single-Site Catalysis: Methane to Methanol Conversion by Fe^{IV}═O. *ACS Catal.* **2018**, *8*, 975−986.

(16) Simons, M. C.; Vitillo, J. G.; Babucci, M.; Hoffman, A. S.; Boubnov, A.; Beauvais, M. L.; Chen, Z.; Cramer, C. J.; Chapman, K. W.; Bare, S. R.; et al. Structure, Dynamics, and Reactivity for Light Alkane Oxidation of Fe(II) Sites Situated in the Nodes of a Metal−Organic Framework. *J. Am. Chem. Soc.* **2019**, *141*, 18142−18151.

(17) Rogge, S. M. J.; Bavykina, A.; Hajek, J.; Garcia, H.; Olivos-Suarez, A. I.; Sepulveda-Escribano, A.; Vimont, A.; Clet, G.; Bazin, P.; Kapteijn, F.; et al. Metal-organic and covalent organic frameworks as single-site catalysts. *Chem. Soc. Rev.* **2017**, *46*, 3134−3184.

(18) Bernales, V.; Ortuño, M. A.; Truhlar, D. G.; Cramer, C. J.; Gagliardi, L. Computational Design of Functionalized Metal−Organic Framework Nodes for Catalysis. *ACS Cent. Sci.* **2018**, *4*, 5−19.

(19) Guesh, K.; Caiuby, C. A. D.; Mayoral, Á.; Díaz-García, M.; Díaz, I.; Sanchez-Sanchez, M. Sustainable Preparation of MIL-100(Fe) and Its Photocatalytic Behavior in the Degradation of Methyl Orange in Water. *Cryst. Growth Des.* **2017**, *17*, 1806−1813.
(20) Skobelev, I. Y.; Sorokin, A. B.; Kovalenko, K. A.; Fedin, V. P.; Kholdeeva, O. A. Solvent-free allylic oxidation of alkenes with O_2 mediated by Fe- and Cr-MIL-101. *J. Catal.* **2013**, *298*, 61−69.
(21) Maksimchuk, N. V.; Zalomaeva, O. V.; Skobelev, I. Y.; Kovalenko, K. A.; Fedin, V. P.; Kholdeeva, O. A. *Proc. R. Soc. London, Ser. A* **2012**, *468*, 2017−2034.
(22) Taylor-Pashow, K. M. L.; Della Rocca, J.; Xie, Z.; Tran, S.; Lin, W. Postsynthetic Modifications of Iron-Carboxylate Nanoscale Metal−Organic Frameworks for Imaging and Drug Delivery. *J. Am. Chem. Soc.* **2009**, *131*, 14261−14263.
(23) Wang, D.; Wang, M.; Li, Z. Fe-Based Metal−Organic Frameworks for Highly Selective Photocatalytic Benzene Hydroxylation to Phenol. *ACS Catal.* **2015**, *5*, 6852−6857.
(24) Dhakshinamoorthy, A.; Alvaro, M.; Horcajada, P.; Gibson, E.; Vishnuvarthan, M.; Vimont, A.; Grenèche, J.-M.; Serre, C.; Daturi, M.; Garcia, H. Comparison of Porous Iron Trimesates Basolite F300 and MIL-100(Fe) As Heterogeneous Catalysts for Lewis Acid and Oxidation Reactions: Roles of Structural Defects and Stability. *ACS Catal.* **2012**, *2*, 2060−2065.
(25) Kholdeeva, O. A.; Skobelev, I. Y.; Ivanchikova, I. D.; Kovalenko, K. A.; Fedin, V. P.; Sorokin, A. B. Hydrocarbon oxidation over Fe- and Cr-containing metal-organic frameworks MIL-100 and MIL-101−a comparative study. *Catal. Today* **2014**, *238*, 54−61.
(26) Santiago-Portillo, A.; Navalón, S.; Cirujano, F. G.; Xamena, F. X. L. i.; Alvaro, M.; Garcia, H. MIL-101 as Reusable Solid Catalyst for Autoxidation of Benzylic Hydrocarbons in the Absence of Additional Oxidizing Reagents. *ACS Catal.* **2015**, *5*, 3216−3224.
(27) Barona, M.; Ahn, S.; Morris, W.; Hoover, W.; Notestein, J. M.; Farha, O. K.; Snurr, R. Q. Computational Predictions and Experimental Validation of Alkane Oxidative Dehydrogenation by Fe_2M MOF Nodes. *ACS Catal.* **2020**, *10*, 1460−1469.
(28) Vitillo, J. G.; Bhan, A.; Cramer, C. J.; Lu, C. C.; Gagliardi, L. Quantum Chemical Characterization of Structural Single Fe(II) Sites in MIL-Type Metal−Organic Frameworks for the Oxidation of Methane to Methanol and Ethane to Ethanol. *ACS Catal.* **2019**, *9*, 2870−2879.
(29) Barona, M.; Snurr, R. Q. Exploring the Tunability of Trimetallic MOF Nodes for Partial Oxidation of Methane to Methanol. *ACS Appl. Mater. Interfaces* **2020**, *12*, 28217−28231.
(30) Metiu, H.; Chrétien, S.; Hu, Z.; Li, B.; Sun, X. Chemistry of Lewis Acid−Base Pairs on Oxide Surfaces. *J. Phys. Chem. C* **2012**, *116*, 10439−10450.
(31) McFarland, E. W.; Metiu, H. Catalysis by Doped Oxides. *Chem. Rev.* **2013**, *113*, 4391−4427.
(32) Li, S.; Wang, Y.; Wu, T.; Schneider, W. F. First-Principles Analysis of Site- and Condition-Dependent Fe Speciation in SSZ-13 and Implications for Catalyst Optimization. *ACS Catal.* **2018**, *8*, 10119−10130.
(33) Li, F.-L.; Wang, P.; Huang, X.; Young, D. J.; Wang, H.-F.; Braunstein, P.; Lang, J.-P. *Angew. Chem., Int. Ed.* **2019**, *58*, 7051−7056.
(34) Abednatanzi, S.; Gohari Derakhshandeh, P.; Depauw, H.; Coudert, F.-X.; Vrielinck, H.; Van Der Voort, P.; Leus, K. *Chem. Soc. Rev.* **2019**, *48*, 2535−2565.
(35) Ko, N.; Choi, P. G.; Hong, J.; Yeo, M.; Sung, S.; Cordova, K. E.; Park, H. J.; Yang, J. K.; Kim, J. Tailoring the water adsorption properties of MIL-101 metal−organic frameworks by partial functionalization. *J. Mater. Chem. A* **2015**, *3*, 2057−2064.
(36) Liao, P.; Getman, R. B.; Snurr, R. Q. Optimizing Open Iron Sites in Metal−Organic Frameworks for Ethane Oxidation: A First-Principles Study. *ACS Appl. Mater. Interfaces* **2017**, *9*, 33484−33492.
(37) Akiyama, G.; Matsuda, R.; Sato, H.; Hori, A.; Takata, M.; Kitagawa, S. Effect of functional groups in MIL-101 on water sorption behavior. *Microporous Mesoporous Mater.* **2012**, *157*, 89−93.
(38) Guo, M.; Corona, T.; Ray, K.; Nam, W. Heme and Nonheme High-Valent Iron and Manganese Oxo Cores in Biological and Abiological Oxidation Reactions. *ACS Cent. Sci.* **2019**, *5*, 13−28.
(39) Huang, X.; Groves, J. T. *JBIC, J. Biol. Inorg. Chem.* **2017**, *22*, 185−207.
(40) Zee, D. Z.; Nippe, M.; King, A. E.; Chang, C. J.; Long, J. R. Tuning Second Coordination Sphere Interactions in Polypyridyl−Iron Complexes to Achieve Selective Electrocatalytic Reduction of Carbon Dioxide to Carbon Monoxide. *Inorg. Chem.* **2020**, *59*, 5206−5217.
(41) Rosen, A. S.; Notestein, J. M.; Snurr, R. Q. High-Valent Metal−Oxo Species at the Nodes of Metal−Triazolate Frameworks: The Effects of Ligand Exchange and Two-State Reactivity for C−H Bond Activation. *Angew. Chem., Int. Ed.* **2020**, *59*, 19494−19502.
(42) Borovik, A. S. Bioinspired Hydrogen Bond Motifs in Ligand Design: The Role of Noncovalent Interactions in Metal Ion Mediated Activation of Dioxygen. *Acc. Chem. Res.* **2005**, *38*, 54−61.
(43) Shook, R. L.; Borovik, A. S. Role of the Secondary Coordination Sphere in Metal-Mediated Dioxygen Activation. *Inorg. Chem.* **2010**, *49*, 3646−3660.
(44) de Visser, S. P.; Ogliaro, F.; Sharma, P. K.; Shaik, S. What Factors Affect the Regioselectivity of Oxidation by Cytochrome P450? A DFT Study of Allylic Hydroxylation and Double Bond Epoxidation in a Model Reaction. *J. Am. Chem. Soc.* **2002**, *124*, 11809−11826.
(45) Frisch, M. J.; Trucks, G. W.; Schlegel, H. B.; Scuseria, G. E.; Robb, M. A.; Cheeseman, J. R.; Scalmani, G.; Barone, V.; Petersson, G. A.; Nakatsuji, H., et al. *Gaussian 16*, rev. B.01; Wallingford, CT, 2016.
(46) Zhao, Y.; Truhlar, D. G. The M06 suite of density functionals for main group thermochemistry, thermochemical kinetics, noncovalent interactions, excited states, and transition elements: two new functionals and systematic testing of four M06-class functionals and 12 other functionals. *Theor. Chem. Acc.* **2008**, *120*, 215−241.
(47) Weigend, F. Accurate Coulomb-fitting basis sets for H to Rn. *Phys. Chem. Chem. Phys.* **2006**, *8*, 1057−1065.
(48) Weigend, F.; Ahlrichs, R. Balanced basis sets of split valence, triple zeta valence and quadruple zeta valence quality for H to Rn: Design and assessment of accuracy. *Phys. Chem. Chem. Phys.* **2005**, *7*, 3297−3305.
(49) Lebedev, O. I.; Millange, F.; Serre, C.; Van Tendeloo, G.; Férey, G. First Direct Imaging of Giant Pores of the Metal−Organic Framework MIL-101. *Chem. Mater.* **2005**, *17*, 6525−6527.
(50) Bonnefoy, J.; Legrand, A.; Quadrelli, E. A.; Canivet, J.; Farrusseng, D. Enantiopure Peptide-Functionalized Metal−Organic Frameworks. *J. Am. Chem. Soc.* **2015**, *137*, 9409−9416.
(51) Anderson, S. L.; Stylianou, K. C. Biologically derived metal organic frameworks. *Coord. Chem. Rev.* **2017**, *349*, 102−128.
(52) Chen, P.; Cabrito, I.; Moura, J. J. G.; Moura, I.; Solomon, E. I. Spectroscopic and Electronic Structure Studies of the μ_4-Sulfide Bridged Tetranuclear CuZ Cluster in N_2O Reductase: Molecular Insight into the Catalytic Mechanism. *J. Am. Chem. Soc.* **2002**, *124*, 10497−10507.
(53) Brown, K.; Tegoni, M.; Prudêncio, M.; Pereira, A. S.; Besson, S.; Moura, J. J.; Moura, I.; Cambillau, C. A novel type of catalytic copper cluster in nitrous oxide reductase. *Nat. Struct. Biol.* **2000**, *7*, 191−195.
(54) Boys, S. F.; Bernardi, F. The calculation of small molecular interactions by the differences of separate total energies. Some procedures with reduced errors. *Mol. Phys.* **1970**, *19*, 553−566.
(55) De Moor, B. A.; Reyniers, M.-F.; Marin, G. B. Physisorption and chemisorption of alkanes and alkenes in H-FAU: a combined ab initio−statistical thermodynamics study. *Phys. Chem. Chem. Phys.* **2009**, *11*, 2939−2958.
(56) Grimme, S. Supramolecular Binding Thermodynamics by Dispersion-Corrected Density Functional Theory. *Chem. - Eur. J.* **2012**, *18*, 9955−9964.
(57) Ribeiro, R. F.; Marenich, A. V.; Cramer, C. J.; Truhlar, D. G. Use of Solution-Phase Vibrational Frequencies in Continuum Models for the Free Energy of Solvation. *J. Phys. Chem. B* **2011**, *115*, 14556−14562.
(58) Zhao, Y.; Truhlar, D. G. Computational characterization and modeling of buckyball tweezers: density functional study of concave-convex $\pi\cdots\pi$ interactions. *Phys. Chem. Chem. Phys.* **2008**, *10*, 2813−2818.
(59) John, M.; Alexopoulos, K.; Reyniers, M.-F.; Marin, G. B. Mechanistic insights into the formation of butene isomers from 1-

https://dx.doi.org/10.1021/acscatal.0c03906
ACS Catal. 2021, 11, 579−589

butanol in H-ZSM-5: DFT based microkinetic modelling. *Catal. Sci. Technol.* **2017**, *7*, 1055−1072.
(60) Isley, W., III https://github.com/william-isley-3rd/Comp-Chem-Tools (accessed 2018-06-12).
(61) Marenich, A. V.; Jerome, S. V.; Cramer, C. J.; Truhlar, D. G. Charge Model 5: An Extension of Hirshfeld Population Analysis for the Accurate Description of Molecular Interactions in Gaseous and Condensed Phases. *J. Chem. Theory Comput.* **2012**, *8*, 527−541.
(62) Ritchie, J. P.; Bachrach, S. M. Some methods and applications of electron density distribution analysis. *J. Comput. Chem.* **1987**, *8*, 499−509.
(63) Gaggioli, C. A.; Stoneburner, S. J.; Cramer, C. J.; Gagliardi, L. Beyond Density Functional Theory: The Multiconfigurational Approach To Model Heterogeneous Catalysis. *ACS Catal.* **2019**, *9*, 8481−8502.
(64) Maihom, T.; Choomwattana, S.; Wannakao, S.; Probst, M.; Limtrakul, J. Ethylene Epoxidation with Nitrous Oxide over Fe−BTC Metal−Organic Frameworks: A DFT Study. *ChemPhysChem* **2016**, *17*, 3416−3422.
(65) Vollhardt, K. P. C.; Schore, N. E. *Organic Chemistry, Structure and Function, 6th ed.*; W. H. Freeman and Company: New York, 2011.
(66) Bordwell, F. G. Equilibrium acidities in dimethyl sulfoxide solution. *Acc. Chem. Res.* **1988**, *21*, 456−463.
(67) Lee, H. M.; Singh, N. J.; Kim, K. S. In *Hydrogen Bonding—New Insights*, Grabowski, S. J., Ed. Springer: Dordrecht, the Netherlands, 2006; pp 149−192.
(68) Latimer, A. A.; Kulkarni, A. R.; Aljama, H.; Montoya, J. H.; Yoo, J. S.; Tsai, C.; Abild-Pedersen, F.; Studt, F.; Nørskov, J. K. Understanding trends in C−H bond activation in heterogeneous catalysis. *Nat. Mater.* **2017**, *16*, 225.
(69) Mayer, J. M. Proton-Coupled Electron Transfer: A Reaction Chemist's View. *Annu. Rev. Phys. Chem.* **2004**, *55*, 363−390.
(70) Kulkarni, A. R.; Zhao, Z. J.; Siahrostami, S.; Norskov, J. K.; Studt, F. Cation-exchanged zeolites for the selective oxidation of methane to methanol. *Catal. Sci. Technol.* **2018**, *8*, 114−123.
(71) Bauer, S.; Serre, C.; Devic, T.; Horcajada, P.; Marrot, J.; Férey, G.; Stock, N. High-Throughput Assisted Rationalization of the Formation of Metal Organic Frameworks in the Iron(III) Amino-terephthalate Solvothermal System. *Inorg. Chem.* **2008**, *47*, 7568−7576.
(72) Zhang, Z.; Li, X.; Liu, B.; Zhao, Q.; Chen, G. Hexagonal microspindle of NH2-MIL-101(Fe) metal-organic frameworks with visible-light-induced photocatalytic activity for the degradation of toluene. *RSC Adv.* **2016**, *6*, 4289−4295.
(73) Lammert, M.; Bernt, S.; Vermoortele, F.; De Vos, D. E.; Stock, N. Single- and Mixed-Linker Cr-MIL-101 Derivatives: A High-Throughput Investigation. *Inorg. Chem.* **2013**, *52*, 8521−8528.
(74) Vitillo, J. G.; Lescouet, T.; Savonnet, M.; Farrusseng, D.; Bordiga, S. Soft synthesis of isocyanate-functionalised metal−organic frameworks. *Dalton Trans.* **2012**, *41*, 14236−14238.
(75) Groutas, W. C.; Brubaker, M. J.; Zandler, M. E.; Mazo-Gray, V.; Rude, S. A.; Crowley, J. P.; Castrisos, J. C.; Dunshee, D. A.; Giri, P. K. Inactivation of leukocyte elastase by aryl azolides and sulfonate salts. Structure-activity relationship studies. *J. Med. Chem.* **1986**, *29*, 1302−1305.
(76) Hutchby, M.; Houlden, C. E.; Ford, J. G.; Tyler, S. N. G.; Gagné, M. R.; Lloyd-Jones, G. C.; Booker-Milburn, K. I. Hindered Ureas as Masked Isocyanates: Facile Carbamoylation of Nucleophiles under Neutral Conditions. *Angew. Chem., Int. Ed.* **2009**, *48*, 8721−8724.
(77) Sim, H. Y. F.; Lee, H. K.; Han, X.; Koh, C. S. L.; Phan-Quang, G. C.; Lay, C. L.; Kao, Y.-C.; Phang, I. Y.; Yeow, E. K. L.; Ling, X. Y. Concentrating Immiscible Molecules at Solid@MOF Interfacial Nanocavities to Drive an Inert Gas−Liquid Reaction at Ambient Conditions. *Angew. Chem., Int. Ed.* **2018**, *57*, 17058−17062.

https://dx.doi.org/10.1021/acscatal.0c03906
ACS Catal. 2021, 11, 579−589